HOSTED BY
ELSEVIER
Available online at www.sciencedirect.com
ScienceDirect
Soils and Foundations 58 (2018) 534–546
SOILS AND FOUNDATIONS
www.elsevier.com/locate/sandf

Unsaturated elasto-plastic constitutive equations for compacted kaolin under consolidated drained and shearing-infiltration conditions

Harianto Rahardjo *, Nguyen Cong Thang, Yongmin Kim, Eng-Choon Leong

School of Civil and Environmental Engineering, Nanyang Technological University, Singapore

Received 13 March 2017; received in revised form 17 January 2018; accepted 29 January 2018
Available online 9 July 2018

Abstract

Transient process of water flow changes the equilibrium conditions of an unsaturated soil, resulting in volume change of a soil. The volume change alters the hydraulic properties of the soil and thus influences the transient process of water flow through the soil. Therefore, the interactive processes between stress-strain behavior and pore-water pressure are the primary processes affecting the mechanical behavior of unsaturated soils. This paper presents coupled elasto-plastic constitutive equations for unsaturated compacted kaolin under consolidated drained and shearing-infiltration conditions. The study focused on the development of the suction increase (SI) yield curve that incorporates changes in matric suction during transient processes. In addition, the relationship of change in specific water volume with respect to net mean stress and matric suction was also proposed by incorporating the hysteresis of soil-water characteristic curve. The simulated results by the proposed constitutive model were compared with those obtained from isotropically consolidated drained tests and shearing infiltration tests of compacted kaolin to verify the proposed model. The simulated results are in close agreement with the experimental results.

Keywords: Elasto-plastic constitutive model; Matric suction; Soil deformation; Hysteresis; Volume change; Unsaturated soils

1. Introduction

A large number of geotechnical problems involve unsaturated soil zones where the voids between soil particles are filled with air and water. There are many practical situations associated with unsaturated soils that are challenging to geotechnical engineers in the field. When fill materials are compacted or loaded, excess pore-air pressure during compaction or loading will dissipate immediately, meanwhile the excess pore-water pressure will dissipate with time. During and after rainstorms the change in pore-water pressure caused by rain water infiltration may result in deformation and instability (Kim et al., 2016)

In the last few decades, a number of theoretical frameworks and constitutive relations based on elasto-plastic theory have been proposed to describe the mechanical behavior of unsaturated soils. These models are capable of reproducing important behavior of unsaturated soils. Alonso et al. (1987, 1990) proposed a general constitutive framework for unsaturated soils. This model was further refined by Toll (1990), Thomas and He (1994), Cui and Delage (1996), Wheeler (1996), Bolzon et al. (1996), Rampino et al. (1999), Simoni and Schrefler (2001), Tang and Graham (2002), Chiu and Ng, 2003, and Thu et al. (2007a). These models were developed based on the independent stress state variables, net normal stress ($\sigma - u_a$) and matric suction ($u_a - u_w$) where σ is the total stress, u_a is the pore-air pressure and u_w is the pore-water pressure. On the other hand, there are different assumptions and different constitutive relationships used in these models.

Peer review under responsibility of The Japanese Geotechnical Society.
* Corresponding author.
E-mail address: chrahardjo@ntu.edu.sg (H. Rahardjo).

https://doi.org/10.1016/j.sandf.2018.02.019
0038-0806/

Wheeler and Sivakumar (1995) proposed an elastoplastic model that is similar to the model of Alonso et al. (1990) but proposed specific water volume as one of the stress state variables for unsaturated soil. Tang and Graham (2002) pointed out that these models are generally developed based on tests on silts, silty clays, or low-plasticity clays such as kaolinite at relatively low and/or constant matric suction. Therefore, it may be termed as a "constant-suction model" and may not provide a complete description of the behavior of compacted, highly plastic soils (Tang and Graham, 2002). Therefore, it would be appropriate to develop elasto-plastic constitutive relations for unsaturated soils that are applicable to a wider range of soil types and boundary conditions.

It has been highlighted that matric suction is an important stress state variable that has a significant influence on yield behavior of unsaturated soils (Fredlund et al., 1996; Vanapalli et al., 1996). Changes in matric suction affect the stress-strain behavior, volume change, and unsaturated shear strength by changing the hydraulic properties of the soil. Thus, many researchers suggested yield loci to define the relation between net mean stress and matric suction. It was noticed that collapse of the soil was closely related to both drying and wetting processes due to the reasons mostly associated with climatic conditions (i.e., rainwater infiltration or evaporation) (Alonso et al., 1990; Wheeler and Sivakumar, 1995).

The main objective of this paper is to present coupled elasto-plastic constitutive equations for unsaturated soil under consolidated drained and shearing-infiltration conditions. The study focused on the development of the suction increase (SI) yield curve that incorporates changes in matric suction during transient processes. In addition, the relationship of change in specific water volume with respect to net mean stress and matric suction was also proposed by incorporating the hysteresis of soil-water characteristic curve. The simulated results by the proposed constitutive model were compared with the experimental results obtained in this study to verify the proposed model.

Statically compacted kaolin specimens were used in this study to carry out the isotropic consolidation tests under different matric suctions, tests for obtaining soil-water characteristic curves under different net mean stresses, consolidated drained triaxial tests, and shearing-infiltration tests for verification of the proposed model.

2. Background for elasto-plastic constitutive relations

An unsaturated soil consists of four phases. When stress gradients are applied, two phases will flow (i.e., air phase and water phase), and the other two phases will come to equilibrium (i.e., soil structure and contractile skin). Volume changes associated with the contractile skin can be assumed to be negligible. Hence, the constitutive relationships for the three phases can be formulated by relating volume changes to changes in stress state variables. In most cases, two constitutive relationships are presented to describe the volume changes associated with an unsaturated soil, one relationship for soil structure (in terms of void ratio or volumetric strain) and another relationship for the water phase (in terms of degree of saturation or water content) (Fredlund and Rahardjo, 1993).

The critical state model is an elasto-plastic constitutive model with elastic behavior when the soil state lies inside the yield surface and plastic strains when the soil state reached the yield surface. The yield surface in saturated soils is represented by a yield envelope in $p-q$ space and a corresponding coupled trace in $p-v$ space. For yielding of unsaturated soils, yield surface should be defined in $p-s$ space for isotropic loading. Thus, many researchers suggest their yield loci to define the relation between net mean stress and matric suction. It was noticed that collapse of the soil occurred during both drying and wetting processes (Gens and Alonso, 1992; Wheeler and Sivakumar, 1995). The yield boundary for unsaturated soils proposed by Alonso et al. (1990) is not continuous and it comes from tests under constant matric suction. Therefore, Tang and Graham (2002) suggested a new yield curve called the Loading-collapse and Suction increase Yield (LSY) curves to consider possible coupling of matric suction-induced hardening. Delage and Graham (1995) argued that the Loading Collapse (LC) and Suction Increase (SI) yield curves should perhaps be coupled.

Alonso et al. (1990) proposed an elasto-plastic model with four state variables: net mean stress (p), deviator stress (q), matric suction (s), and specific volume (v). On the other hand, Wheeler (1996), Rampino et al. (2000), Wang et al. (2002) and Chiu and Ng (2003) indicated that specific water volume (v_w) should be taken into account in the elasto-plastic constitutive framework model. The behavior of unsaturated soil can then be described using five state variables under axisymmetric stress conditions as follows:

$$p = \frac{\sigma_1 + \sigma_2 + \sigma_3}{3} - u_a \tag{1}$$

$$q = \sigma_1 - \sigma_3 \tag{2}$$

$$s = u_a - u_w \tag{3}$$

$$v = 1 + e \tag{4}$$

$$v_w = 1 + S \cdot e \tag{5}$$

where σ_1, σ_2, σ_3 = total principal normal stresses; e = void ratio; v_w = specific water volume; and S = degree of saturation.

The total strain increment ($d\varepsilon$) is composed of the elastic strain increment ($d\varepsilon^e$) and the plastic strain increment ($d\varepsilon^p$). Volumetric strain increment ($d\varepsilon_v$) and shear strain increment ($d\varepsilon_q$) can be calculated as follows (Alonso et al., 1990):

$$d\varepsilon_v = d\varepsilon^e_{v(p)} + d\varepsilon^e_{v(s)} + d\varepsilon^p_{v(p)} + d\varepsilon^p_{v(s)} \tag{6}$$

$$d\varepsilon_q = d\varepsilon^e_q + d\varepsilon^p_q \tag{7}$$

where $d\varepsilon^e_{v(p)}$ is the elastic volumetric strain increment induced by changes in mean net stress, $d\varepsilon^e_{v(s)}$ is the elastic

volumetric strain increment induced by changes in matric suction, $d\varepsilon^{p}_{v(p)}$ is the plastic volumetric strain increment induced by changes in net mean stress, $d\varepsilon^{p}_{v(s)}$ is the plastic volumetric strain increment induced by changes in matric suction, $d\varepsilon^{e}_{q}$ is the elastic shear strain increment, and $d\varepsilon^{p}_{q}$ is the plastic shear strain increment.The elastic volumetric strain increment due to the change in net mean stress can be calculated using Eq. (8):

$$d\varepsilon^{e}_{v(p)} = \frac{\kappa}{v}\frac{dp}{p} \tag{8}$$

where κ is the elastic stiffness parameter for changes in net mean stress, dp is the increment of net mean stress. The elastic volumetric strain increment due to changes in matric suction can be calculated using Eq. (9):

$$d\varepsilon^{e}_{v(s)} = \frac{\kappa_s}{v}\frac{ds}{s+p_{at}} \tag{9}$$

where κ_s is the elastic stiffness parameter for changes in matric suction, p_{at} is the atmospheric pressure. The plastic volumetric strain caused by the changes in net mean stress can be calculated using Eq. (10):

$$d\varepsilon^{p}_{v(p)} = \frac{\lambda(s)-\kappa}{v}\frac{dp}{p} \tag{10}$$

where $\lambda(s)$ is the plastic stiffness parameter for changes in net mean stress for a virgin state of soil under a given matric suction. The plastic strain caused by the increment of matric suction can be calculated using Eq. (11):

$$d\varepsilon^{p}_{v(s)} = \frac{\lambda_s-\kappa_s}{v}\frac{ds}{s+p_{at}} \tag{11}$$

where λ_s is the plastic stiffness parameter for changes in matric suction for a virgin state of the soil.

3. Proposed elasto-plastic constitutive equations for unsaturated soils

3.1. Yielding curves in the $p-s$ space

3.1.1. Loading-collapse (LC) yield curve

The loading-collapse (LC) yield curve was derived by considering the response to isotropic loading of two specimens subjected to different matric suctions (s). The stress path and corresponding change in specific volume (Δv) can be related to the changes in net mean stress and matric suction. The relationship of specific volume with respect to net mean stress is shown in Fig. 1(a). The specific volume (v) can be calculated using Eq. (12) (Wheeler and Sivakumar, 1995):

$$v = N(s) - \lambda(s)\ln\left(\frac{p}{p_{at}}\right) \tag{12}$$

where $N(s)$ is the specific volume of the normal consolidation line under a given matric suction.

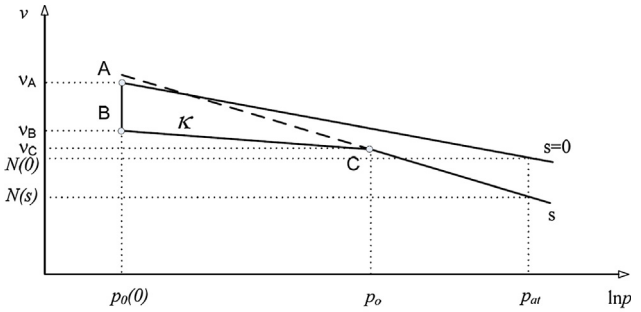

(a) Relationship between specific volume and net mean stress

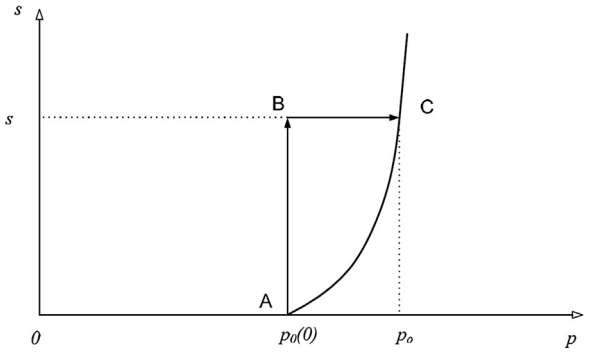

(b) Stress path and yield curve in $p-s$ plane

Fig. 1. Derivation of loading-collapse (LC) yield curve equation.

The equation of the LC yield curve can be derived based on the elastic behavior inside the yield surface. Fig. 1(b) shows the stress path and yield curve in $p-s$ plane. When a stress state moves from point A at zero suction and net mean stress ($p_0(0)$) to a new point C at matric suction (s) and net mean stress (p_0) along the yield curve under an isotropic stress state, the stress path from A to C follows the elastic stress path ABC and the change in specific volume (Δv) can be calculated based on two elastic stiffness parameters κ and κ_s as follows (Alonso et al. 1990):

$$\Delta v = -\kappa_s \ln\left(\frac{s+p_{at}}{p_{at}}\right) - \kappa\ln\left(\frac{p_o}{p_o(0)}\right) \tag{13}$$

where p_o is the mean net yield stress of unsaturated soil, $p_o(0)$ is the mean net yield stress at the saturated condition.

Points A and C not only lie on the yield curve, but they also lie on the corresponding line that relates the specific volume to matric suction for an appropriate value of net mean stress. Therefore, based on Eq. (12) an alternative expression for the change in specific volume between point A and point C can also be calculated as follows (Wheeler and Sivakumar, 1995):

$$\Delta v = N(s) - \lambda(s)\ln\left(\frac{p_o}{p_{at}}\right) - N(0) + \lambda(0)\ln\left(\frac{p_o}{p_{at}}\right) \tag{14}$$

where $N(0)$ is the specific volume of the normal consolidation line under zero matric suction at atmospheric pressure, $\lambda(0)$ is the plastic stiffness parameter from the normally consolidated curve under zero matric suction.

The LC yield curve equation can be obtained by elimination of Δv from Eqs. (13) and (14) as follows:

$$[\lambda(s)-\kappa]\ln\left(\frac{p_o}{p_{at}}\right)=[\lambda(0)-\kappa]\ln\left(\frac{p_o(0)}{p_{at}}\right)+N(s)-N(0)+\kappa_s\ln\left(\frac{s+p_{at}}{p_{at}}\right) \quad (15)$$

3.1.2. Suction increase (SI) yield curve

The equation of the SI yield curve can be derived by considering a variation between specific volume (v) and matric suction (s) at a particular net mean stress (p). When soil matric suction reaches yield suction (s_0), irreversible strain will start to develop. The relationship between specific volume and matric suction as shown in Fig. 2(a) can be expressed as follows:

$$v=N_s(p)-\lambda_s(p)\ln\left(\frac{s}{p_{at}}\right) \quad (16)$$

where $N_s(p)$ is the specific volume under a given net mean stress at matric suction equal to atmospheric pressure.

The equation of the SI yield curve can be derived based on the elastic behavior inside the yield surface. Fig. 2(b) shows the stress path and yield curve in $p-s$ plane. When a stress state moves from point A at net mean stress (p) and matric suction ($s_o(p)$) to a new point C at suction ($s_o(0)$) and zero net mean stress ($p=0$) along the yield curve under an isotropic stress state, the stress path from A to C follows the elastic stress path ABC and the change in specific volume (Δv) can be calculated based on two elastic stiffness parameters κ and κ_s as follows:

$$\Delta v=-\kappa_s\ln\left(\frac{s_o(p)}{s_o(0)}\right)-\kappa\ln\left(\frac{p+p_{at}}{p_{at}}\right) \quad (17)$$

Here, p_{at} has been added to p to avoid infinite values when p approaches zero.

Point A and point C not only lie on the yield curve, but they also lie on the corresponding line that relates the specific volume to matric suction for an appropriate value of net mean stress. Therefore, based on Eq. (16) an alternative expression for the change in specific volume between point A and point C can also be calculated as follows:

$$\Delta v=N_s(p)-\lambda_s(p)\ln\left(\frac{s_o(p)}{p_{at}}\right)-N_s(0)+\lambda_s(0)\ln\left(\frac{s_o(0)}{p_{at}}\right) \quad (18)$$

The SI yield curve equation that is capable of considering the change of matric suction can be obtained by equating Eqs. (17) and (18) as follows:

$$[\lambda_s(p)-\kappa_s]\ln\left(\frac{s_o(p)}{p_{at}}\right)=[\lambda_s(0)-\kappa_s]\ln\left(\frac{s_o(0)}{p_{at}}\right)+N_s(p)-N_s(0)+\kappa\ln\left(\frac{p+p_{at}}{p_{at}}\right) \quad (19)$$

The yield curve on $p-s$ plane is a combination of LC yield curve and SI yield curve. Fig. 3 shows the sketch of the yield curve on $p-s$ plane.

3.2. Yield surface in the $p-q-s$ space

The yield surface in the $p-q-s$ plane would be elliptical as shown in Fig. 4. When the stress path in radial direction of $p-s$ plane reaches the SI yield curve at point D (path OCD) or reaches the LC yield curve at point B (path OAB), the yield curve in q-OAB and q-OCD plane can be expressed as follows, respectively:

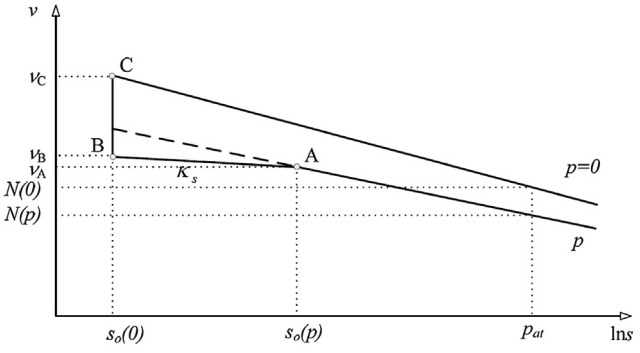

(a) Relationship between specific volume and matric suction

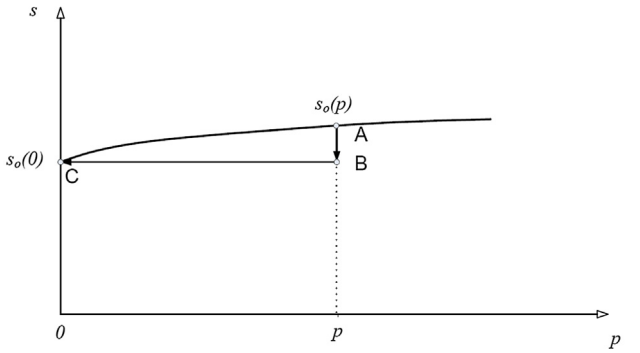

(b) Stress path and yield curve in $p-s$ plane

Fig. 2. Derivation of suction increase (SI) yield curve equation.

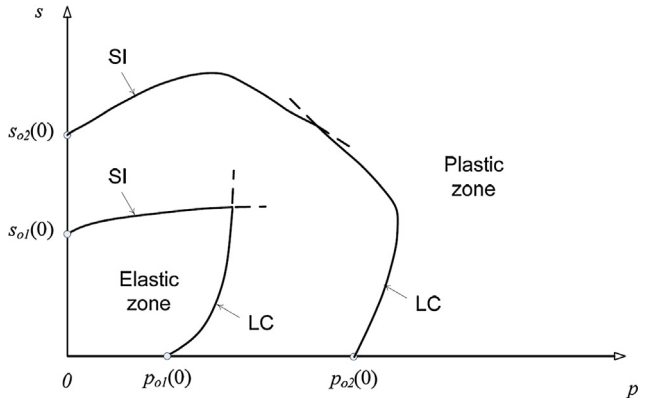

Fig. 3. Combination of loading-collapse (LC) and suction increase (SI) yield curve in $p-s$ plane.

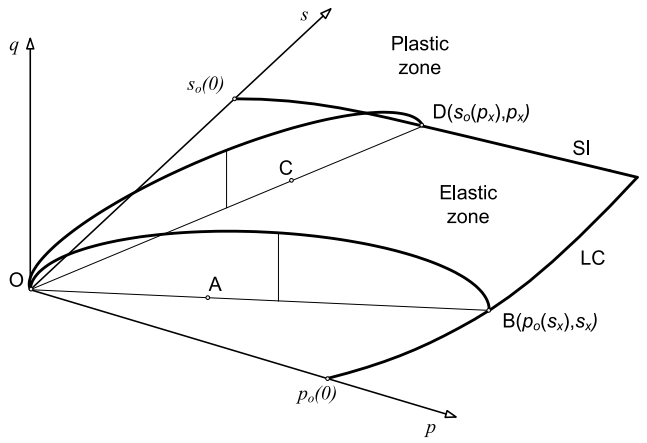

Fig. 4. Loading-collapse (LC) and suction increase (SI) curves, and triaxial stress state in $q-p-s$ space.

$$q^2 = M_*^2\sqrt{p^2+s^2}\left(\sqrt{[p_o(s_x)]^2+s_x^2}-\sqrt{p^2+s^2}\right) \tag{20}$$

$$q^2 = M_*^2\sqrt{p^2+s^2}\left(\sqrt{p_x^2+[s_o(p_x)]^2}-\sqrt{p^2+s^2}\right) \tag{21}$$

where M_* is the ratio between minor and major diameters of the elliptical yield curve, $(p_o(s_x), s_x)$ is the stress state location on the LC yield curve (i.e., point B), $(p_x, s_o(p_x))$ is the stress state location on the SI yield curve (i.e., point D). The ratio M_* is a function of net mean stress and matric suction.

The evolution of yield surface is controlled by the hardening parameters, p_o and s_o (Alonso et al., 1990). The hardening parameters can be calculated based on the total plastic volumetric strain as follows:

$$\frac{dp_o}{p_o} = \frac{v d\varepsilon_v^p}{\lambda(0)-\kappa(0)} \tag{22}$$

$$\frac{ds_o}{s_o} = \frac{v d\varepsilon_v^p}{\lambda_s(0)-\kappa_s(0)} \tag{23}$$

where p_o is the yield stress of saturated soil, $d\varepsilon_v^p$ is the increment of plastic volumetric strain, s_o is the matric suction at yield point.

Gens and Potts (1982) pointed out that the conventional critical state models often overestimated K_o. In order to avoid the overestimation of K_o, the associated flow rule was modified by introducing an α parameter (Ohmaki, 1982). The LC and SI plastic potential functions under non-associated flow rule can be expressed as follows:

$$G^{LC} = \alpha q^2 - M_*^2\sqrt{p^2+s^2}\left(\sqrt{[p_o(s_x)]^2+s_x^2}-\sqrt{p^2+s^2}\right) = 0 \tag{24}$$

$$G^{SI} = \alpha q^2 - M_*^2\sqrt{p^2+s^2}\left(\sqrt{p_x^2+[s_o(p_x)]^2}-\sqrt{p^2+s^2}\right) = 0 \tag{25}$$

where α is the soil parameter which can be calculated as follows:

$$\alpha = \frac{M(M-9)(M-3)}{9(6-M)}\frac{1}{1-\frac{\kappa(0)}{\lambda(0)}} \tag{26}$$

The LC and SI yield surfaces that are presented in Eqs. (20) and (21) can be rewritten as follows:

$$F^{LC} = q^2 - M_*^2\sqrt{p^2+s^2}\left(\sqrt{[p_o(s_x)]^2+s_x^2}-\sqrt{p^2+s^2}\right) = 0 \tag{27}$$

$$F^{SI} = q^2 - M_*^2\sqrt{p^2+s^2}\left(\sqrt{p_x^2+[s_o(p_x)]^2}-\sqrt{p^2+s^2}\right) = 0 \tag{28}$$

The plastic potential functions are presented in Eqs. (24) and (25). The hardening laws are presented in Eqs. (22) and (23). Plastic strain increment can be calculated based on flow rules as follows:

$$d\varepsilon^p = \left(\frac{\partial G^{LC}}{\partial\sigma}+\frac{\partial G^{LC}}{\partial s}\right)d\lambda^{LC} + \left(\frac{\partial G^{SI}}{\partial\sigma}+\frac{\partial G^{SI}}{\partial s}\right)d\lambda^{SI} \tag{29}$$

where λ^{LC} and λ^{SI} are the non-negative plastic multipliers. In order to ensure that the stress state remains on the yield surface, the consistency condition can be written as follows:

$$\frac{\partial F^{LC}}{\partial\sigma}d\sigma + \frac{\partial F^{LC}}{\partial s}ds + \frac{\partial F^{LC}}{\partial p_o}\frac{\partial p_o}{\partial p_o(0)}dp_o(0) + \frac{\partial F^{LC}}{\partial p_o}\frac{\partial p_o}{\partial s}ds + \frac{\partial F^{LC}}{\partial p_o}\frac{\partial p_o}{\partial\varepsilon_v^p}d\varepsilon_v^p = 0 \tag{30}$$

$$\frac{\partial F^{SI}}{\partial\sigma}d\sigma + \frac{\partial F^{SI}}{\partial s}ds + \frac{\partial F^{SI}}{\partial s_o}\frac{\partial s_o}{\partial s_o(0)}ds_o(0) + \frac{\partial F^{SI}}{\partial s_o}\frac{\partial s_o}{\partial p}dp + \frac{\partial F^{SI}}{\partial s_o}\frac{\partial s_o}{\partial\varepsilon_v^p}d\varepsilon_v^p = 0 \tag{31}$$

The total strain increment ($d\varepsilon$) is the sum of the elastic strain increment ($d\varepsilon^e$) and the plastic increment ($d\varepsilon^p$). Elastic strain increment can be calculated based on Eq. (29) as follows:

$$d\varepsilon^e = d\varepsilon - \left(\frac{\partial G^{LC}}{\partial\sigma}+\frac{\partial G^{LC}}{\partial s}\right)d\lambda^{LC} - \left(\frac{\partial G^{SI}}{\partial\sigma}+\frac{\partial G^{SI}}{\partial s}\right)d\lambda^{SI} \tag{32}$$

Incremental stress-strain relation can be calculated as follows:

$$d\sigma = D^e d\varepsilon^e - \mathrm{h}^e ds \tag{33}$$

where D^e is the elasticity tensor and h^e is the hardening parameter related to the elastic hardening modulus. Substituting Eq. (32) into Eq. (33) gives,

$$d\sigma = D^e\left(d\varepsilon - \left(\frac{\partial G^{LC}}{\partial\sigma}+\frac{\partial G^{LC}}{\partial s}\right)d\lambda^{LC} - \left(\frac{\partial G^{SI}}{\partial\sigma}+\frac{\partial G^{SI}}{\partial s}\right)d\lambda^{SI}\right) - \mathrm{h}^e ds \tag{34}$$

Substituting Eq. (34) into Eqs. (30) and (31) yields the following equations:

$$\frac{\partial F^{LC}}{\partial \sigma}\left[D^e\left(d\varepsilon-\left(\frac{\partial G^{LC}}{\partial \sigma}+\frac{\partial G^{LC}}{\partial s}\right)d\lambda^{LC}-\left(\frac{\partial G^{SI}}{\partial \sigma}+\frac{\partial G^{SI}}{\partial s}\right)d\lambda^{SI}\right)-\mathrm{h}^e ds\right]+\frac{\partial F^{LC}}{\partial s}ds+\frac{\partial F^{LC}}{\partial p_o}\frac{\partial p_o}{\partial p_o(0)}dp_o(0)+\frac{\partial F^{LC}}{\partial p_o}\frac{\partial p_o}{\partial s}ds+\frac{\partial F^{LC}}{\partial p_o}\frac{\partial p_o}{\partial \varepsilon_v^p}d\varepsilon_v^p=0 \quad (35)$$

$$\frac{\partial F^{SI}}{\partial \sigma}\left[D^e\left(d\varepsilon-\left(\frac{\partial G^{LC}}{\partial \sigma}+\frac{\partial G^{LC}}{\partial s}\right)d\lambda^{LC}-\left(\frac{\partial G^{SI}}{\partial \sigma}+\frac{\partial G^{SI}}{\partial s}\right)d\lambda^{SI}\right)-\mathrm{h}^e ds\right]+\frac{\partial F^{SI}}{\partial s}ds+\frac{\partial F^{SI}}{\partial s_o}\frac{\partial s_o}{\partial s_o(0)}ds_o(0)+\frac{\partial F^{SI}}{\partial s_o}\frac{\partial s_o}{\partial p}dp+\frac{\partial F^{SI}}{\partial s_o}\frac{\partial s_o}{\partial \varepsilon_v^p}d\varepsilon_v^p=0 \quad (36)$$

For the case when the stress state is located on both LC and SI yield surfaces, Eqs. (35) and (36) can be solved to obtain the plastic multiplier ($d\lambda^{LC}$ and $d\lambda^{SI}$). For the case when the stress state is located on LC yield surface ($d\lambda^{SI}=0$), Eq. (35) can be solved to obtain $d\lambda^{LC}$. For the case when the stress state is located on SI yield surface ($d\lambda^{LC}=0$), Eq. (36) can be solved to obtain $d\lambda^{SI}$.

Substituting $d\lambda^{LC}$ and $d\lambda^{SI}$ into Eq. (34) yields the incremental stress-strain relations.

$$d\sigma = D^{ep}d\varepsilon - \mathrm{h}^{ep}ds \quad (37)$$

where D^{ep} is the elasto-plasticity tensor and h^{ep} is the hardening parameter related to the elasto-plastic hardening modulus.

3.3. Water phase constitutive equations

The relationship between specific water volume (ν_w) and net mean stress (p) at a certain matric suction proposed by Wheeler (1996) and modified by Thu et al. (2007b) was adopted. The idealized relationship is presented in Fig. 5. By taking into account the effect of unloading path (i.e. stress state located in the elastic region), the change in specific water volume with respect to the change in net mean stress can be calculated as follows:

$$dv_w = -[\lambda_w(s)-\kappa_w(s)]\frac{dp_o}{p_o}-\kappa_w(s)\frac{dp}{p} \quad (38)$$

where $\lambda_w(s)$ is the plastic compressibility index with respect to water phase and $\kappa_w(s)$ is the elastic compressibility index with respect to water phase.

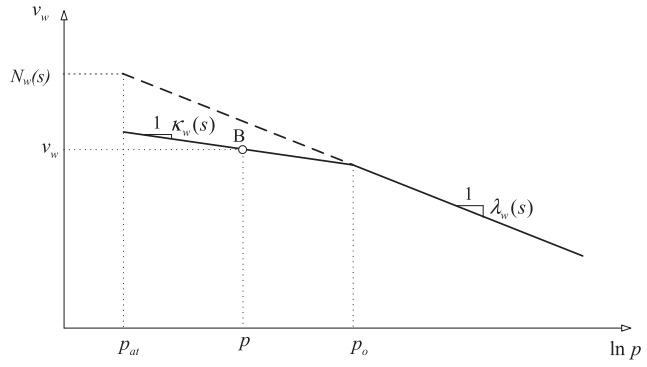

Fig. 5. The idealized relationship between specific water volume and net mean stress at a constant matric suction (modified after Wheeler, 1996; Thu et al., 2007b).

The relationship between volumetric water content (θ_w) or degree of saturation (S) and matric suction (s) is commonly referred to as the soil-water characteristic curve (SWCC) as shown in Fig. 6(a). The relationship between volumetric water content and logarithmic matric suction can be assumed as a piecewise linear function.

$$dS = \lambda_{SWCC}\frac{ds}{s} \quad (39)$$

where λ_{swcc} is the slope of the SWCC.

When matric suction is increased from zero until saturation suction (s_{sa}), degree of saturation remains constant (Fig. 6b). The degree of saturation decreases rapidly when matric suction is increased from the air-entry value (s_{ae}) until it reaches the residual suction (s_{re}). The slope of the SWCC is assumed to be constant between the air-entry value and the residual suction. When matric suction is increased from the residual suction to 1 GPa, degree of saturation decreases from the residual degree of saturation to zero (Fredlund and Rahardjo, 1993). To account for hysteresis, drying and wetting of soil-water characteristic curves were considered in this study. For matric suctions greater than the residual soil suction (s_{re}) and lower than the saturation suction (s_{sa}), wetting and drying curves coincide with each other (paths AB and EF in Fig. 6b). Slope of the wetting curve (λ_{ws}) for matric suction from the water-entry value to the saturation suction is assumed to be the same as the slope of the drying curve from the air-entry value to the residual suction. Slopes (κ_{ws}) for the change

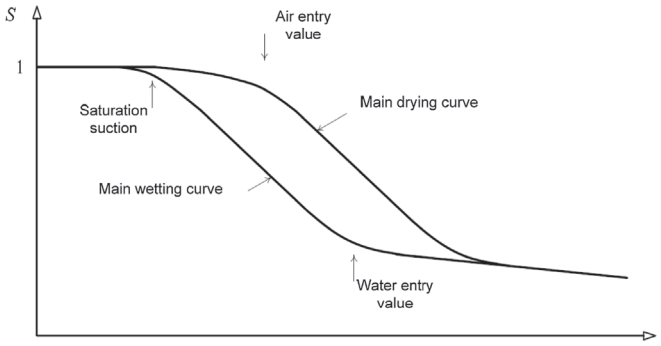

(a) Typical soil-water characteristic curve (SWCC)

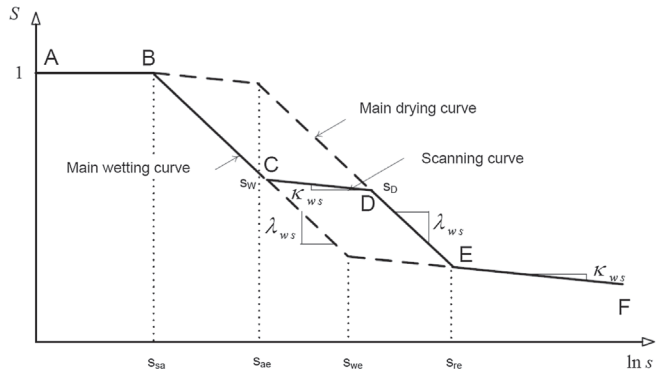

(b) Idealized SWCC (solid lines represent current SWCC) (Modified after Sheng et al. 2008)

Fig. 6. Relationship between degree of saturation and matric suction.

from wetting curve to drying curve and vice versa are represented by scanning curves.

In this study, a typical SWCC (Fig. 6a) is simplified as an idealized SWCC (Fig. 6b). Slope of the scanning curves, slope of the drying curve from the saturation suction to the air-entry value and slope of the wetting curve for matric suctions higher than the water-entry value are considered equal. This simplified SWCC is similar to the model presented by Wheeler et al. (2003) and Sheng et al. (2008).

An unsaturated state always lies within the main drying and wetting curves. Drying or wetting within the hysteresis loop follows the scanning curve until matric suction reaches the main drying or wetting curve. Once matric suction reaches the main drying at S_D or wetting curve at S_W, further drying or wetting will follow the main drying or wetting curve, respectively. The main wetting curve is for matric suction from zero to S_W; the scanning curve is for matric suction from S_W to S_D; and the main drying curve for matric suction is from S_D to 1 GPa. In this study, it can be called "current SWCC" (i.e. path ABCDEF in Fig. 6b). Slope of the current SWCC is determined as follows:

$$\lambda_{SWCC} = \begin{cases} 0 & s < s_{sa} \\ \lambda_{ws} & s_{sa} < s < s_W \\ \kappa_{ws} & s_W < s < s_D \\ \lambda_{ws} & s_D < s < s_{re} \\ \kappa_{ws} & s \geqslant s_{re} \end{cases} \tag{40}$$

The variation of specific water volume with respect to matric suction can be obtained based on Eqs. (5) and (39) as follows:

$$dv_w = (\lambda_{SWCC} e + \kappa_s S)\frac{ds}{s} + \lambda_s S \frac{ds_o}{s_o} \tag{41}$$

where κ_s is the elastic stiffness parameter for changes in matric suction, e is the void ratio and S is the degree of saturation. Based on Eqs. (38) and (41), the change in specific water volume with respect to net mean stress and matric suction can be expressed as follows:

$$dv_w = -[\lambda_w(s) - \kappa_w(s)]\frac{dp_o}{p_o} - \kappa_w(s)\frac{dp}{p} + (\lambda_{SWCC} e + \kappa_s S)\frac{ds}{s} + \lambda_s S \frac{ds_o}{s_o} \tag{42}$$

4. Model prediction and comparison with experimental results

The proposed model was used to simulate the response of unsaturated soil specimen during shearing under consolidated drained and shearing-infiltration conditions (i.e., the two stress paths that commonly occur in the field). The soil parameters for the model prediction were obtained from SWCC tests under different net mean stresses and isotropic consolidation tests under different matric suctions. The agreements between the results of simulations and experiments provide the verifications for the proposed model.

4.1. Specimen preparation and testing programme

The soil used in the experimental program was kaolin from Kaolin Malaysia SDN BHD. The index properties of the kaolin are presented in Table 1. Compacted specimens at a dry density of 1.35 Mg/m^3 and a water content of 21.7% were used in the experiments. The dimensions of the specimen were 100 mm in height and 50 mm in diameter. The static compaction method was used in order to obtain identical specimens with a uniform density along the specimen (Reddy and Jagadish, 1993).

The test procedures for triaxial tests given by Head (1986) and the procedures for controlling pore-air pressure in unsaturated soil testing given by Fredlund and Rahardjo (1993) were adopted in the experiments. The axis translation technique (Hilf, 1956) was used for establishing the initial matric suction of the specimen. The testing procedures for isotropic consolidation tests and SWCC tests given by Thu et al. (2007b) were adopted in this study. In addition, the testing procedures for shearing tests under consolidated drained conditions given by Thu et al. (2007c) and for shearing tests under shearing-infiltration conditions given by Meilani et al. (2005) were also adopted in this study.

SWCC tests at net mean stresses of 10, 50, 100 and 250 kPa (i.e., SWCC-10, SWCC-50, SWCC 100, and SWCC-250) were conducted to obtain air-entry value, yield suction (s_o), and stiffness parameters ($N_s(p)$, $\lambda_s(p)$,$\kappa_s(p)$). The variations of specific volume, specific water volume, and volumetric water content with respect to matric suction of specimen SWCC-10 are illustrated in Fig. 7. The specific volume ($v = 1 + e$) decreases as matric suction increases. Matric suction at the point where specific volume starts to decrease drastically (i.e. inflection point) is called yield suction (s_o) of soil specimen (Alonso et al., 1990). The volumetric water content (i.e., the ratio between volume of water and total volume of soil, $\theta_w = V_w/V$) also decreases as matric suction increases. The value of matric suction at which air first enters the pore of soil is called air-entry value (AEV). The AEV and yield suction increase as net mean stress increases. The specific volume on the virgin curve of the isotropic suction consolidation curve at reference matric suction of 100 kPa (i.e., $N_s(p)$) also varies with

Table 1
Index properties of compacted kaolin.

Soil properties	Value
Specific gravity, G_s	2.68
Liquid limit, LL (%)	56
Plastic limit, PL (%)	38
Plastic index, PI (%)	18
Clay (%)	16.3
Silt (%)	83.7
Unified Soil Classification System (USCS)	MH
Maximum dry density, ρ_{drymax} (Mg/m^3)	1.37
Optimum water content, w_{opt} (%)	26.5

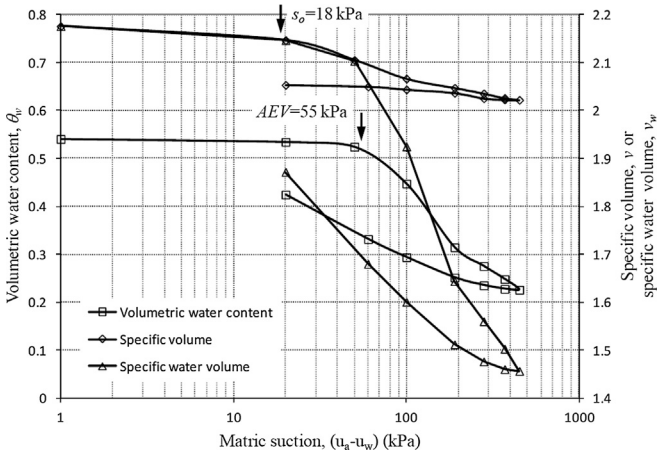

Fig. 7. Variations of volumetric water content, specific volume and specific water volume with respect to matric suction of specimen SWCC-10.

Table 2
Summary of parameters obtained from SWCC tests on compacted kaolin.

Net mean stress, p (kPa)	AEV (kPa)	$N_s(p)$	$\lambda_s(p)$	$\kappa_s(p)$	s_o (kPa)
10	55	2.075	0.044	0.009	18.0
50	60	2.056	0.026	0.007	18.5
100	71	2.031	0.020	0.004	21.8
250	91	1.976	0.020	0.004	32.5

net mean stress. At net mean stress of 10 kPa, the $N_s(10)$ has a value of 2.075, which decreases with the increase in net mean stress. Similarly, the slope of the virgin curve ($\lambda_s(p)$) and unloading/reloading curves ($\kappa_s(p)$) of the isotropic suction consolidation curve decreases with the increase in net mean stress. The soil parameters obtained from the SWCC tests are summarized in Table 2.

Isotropic consolidation tests at matric suctions of 0, 30, 150 and 300 kPa (i.e., IC-0, IC-30, IC-150, and IC-300) were conducted to obtain yield stress (p_o) and stiffness parameters such as $N(s)$, $N_w(s)$, $\lambda(s)$, $\kappa(s)$. The variation of specific volume ($v = 1 + e$) and specific water volume ($v_w = 1 + Se$) with respect to net mean stress at various matric suctions are shown in Figs. 8 and 9, respectively.

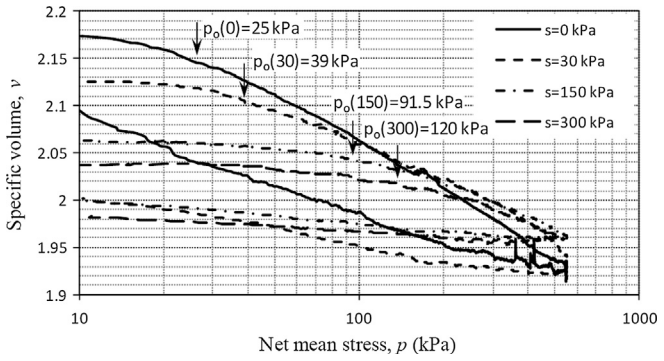

Fig. 8. Specific volume versus net mean stresses at different matric suctions.

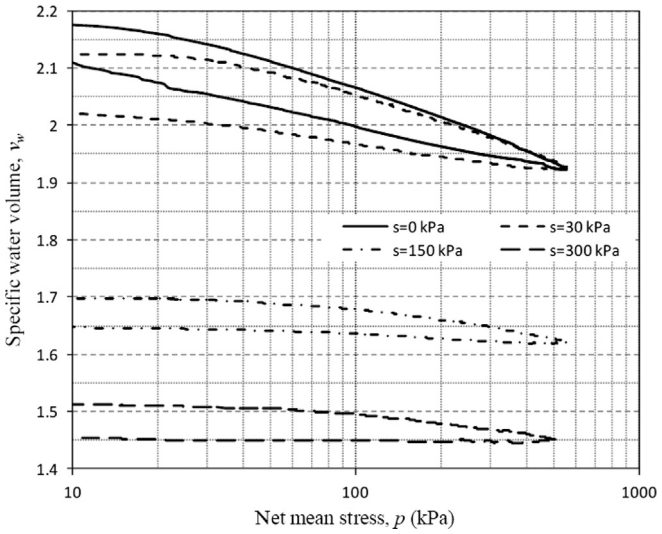

Fig. 9. Specific water volume versus net mean stresses at different matric suctions.

Fig. 8 shows specific volume decreases rapidly when the net mean stress reaches yield stress. The yield stress increases as the matric suction increases. The specific volume on normal consolidation curve at reference net mean stress of 100 kPa (i.e., $N(s)$) varies with matric suction. At saturated condition, the $N(s)$ has a value of 2.052, which decreases with the increase in matric suction. The specific water volume at reference net mean stress of 100 kPa (i.e., $N_w(s)$) has a value of 2.052, which also decreases with the increase in matric suction. Similarly, the slope of the normal consolidation curve ($\lambda(s)$) and unloading/reloading curves ($\kappa(s)$) of the isotropic consolidation curve decreases with the increase in matric suction. The soil parameters obtained from the isotropic consolidation tests are summarized in Table 3.

Consolidated drained (CD) triaxial tests at matric suctions of 0, 100, and 200 kPa under net confining stresses of 100 and 300 kPa were conducted to obtain shear strength parameters. Fig. 10 shows the variation of deviator stress with respect to axial strain during the shearing stage under the same matric suction of 0, 100, and 200 kPa but different net confining stresses (i.e., 100 kPa or 300 kPa). The peak deviator stress was used as failure criterion. The results indicate that the stiffness of the compacted kaolin specimen increases with the increase in net confining stress and matric suction as expected. The shear strength parameters (ϕ' and c') obtained from the extended Mohr-Coulomb failure envelope of the compacted kaolin from the CD triaxial tests at zero matric suction are summarized in Table 4. The angle (ϕ^b), indicating the rate of change in shear strength relative to a change matric suction on the net normal stress of zero-plane, that was obtained from the CD triaxial tests at different matric suction is also presented in Table 4.

Shearing-infiltration triaxial tests at matric suctions of 200 and 300 kPa under net confining stresses of 100, 200,

Table 3
Summary of parameters obtained from isotropic consolidation tests on compacted kaolin.

Matric suction, s (kPa)	$N(s)$	$N_w(s)$	$\lambda(s)$	$\lambda_w(s)$	$\kappa(s)$	$\kappa_w(s)$	p_o (kPa)
0	2.052	2.052	0.071	0.071	0.025	0.025	25.0
30	2.045	2.045	0.068	0.068	0.018	0.018	39.0
150	2.041	1.685	0.046	0.036	0.009	0.006	91.5
300	2.034	1.507	0.044	0.033	0.007	0.004	120.0

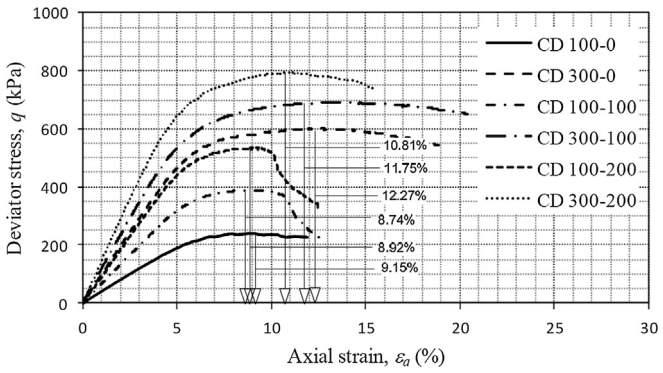

Fig. 10. Peak deviator stresses of the consolidation drained triaxial tests under various matric suctions and net confining stresses.

Table 4
Summary of shear strength parameters obtained from consolidated drained triaxial tests on compacted kaolin.

Parameter	Value
Angle of internal friction associated with net normal stress, ϕ' (°)	25.6
Effective cohesion, c' (kPa)	33.3
Angle indicating rate of change in shear strength relative to matric suction, ϕ^b (°)	21.1

and 300 kPa at the beginning of the shearing stage were conducted. The specimen was sheared up to approximately 80% of the peak shear stress at failure (Han, 1997). In the infiltration stage, a constant deviator stress was maintained by a force actuator while water was injected from the base of the specimen. One set of the test results are presented in Figs. 16–18 to verify the simulated results by the proposed constitutive model.

4.2. Prediction from the proposed model

The initial point for all of the prediction process was at the end of the saturation stage. At this point, the predicted soil specimen has net mean stress (p) of 10 kPa, matric suction (s) of 0 kPa, specific volume (v_i), yield stress (p_o) at matric suction of 0 kPa, and initial yield matric suction (s_o) at net mean stress of 10 kPa.

For the prediction of SWCC test, the elastic strain and plastic strain at the end of the consolidation stage were calculated based on the initial yield stress at matric suction of 0 kPa ($p_{oi}(0)$), Eqs. (8) and (10). The corresponding yield suction at net mean stress of 10 kPa at the end of consolidation stage was calculated based on Eq. (23). Initial loading-collapse (LC) and suction increase (SI) yield curves of the SWCC tests were predicted using Eqs. (15) and (19), respectively.

For the prediction of isotropic consolidation test, the elastic strain and plastic strain at the end of the matric suction equalization stage were calculated based on the initial yield suction at net mean stress of 10 kPa ($s_{oi}(10)$), Eqs. (9) and (11). The corresponding yield stress at the end of matric suction equalization stage was calculated based on Eq. (22). Initial LC and SI yield curves of the isotropic consolidation tests were predicted using Eqs. (15) and (19), respectively.

For the prediction of CD triaxial test, the prediction of consolidation stage was similar to the prediction of SWCC tests and the prediction of matric suction equalization stage was similar to the prediction of isotropic consolidation tests. During the shearing stage, an incremental deviator stress (Δq) of 1 kPa was applied while the confining stress and matric suction were maintained constant. As a result, the increment in net mean stress was 1/3 kPa. For each loading step, the corresponding yield stress and the yield suction at isotropic stage were calculated based on the consistency condition (i.e., Eqs. (30) and (31)). The prediction stopped when the axial strain increased rapidly, indicating failure condition. The LC and SI yield curves at the beginning of the shearing stage (i.e., at the end of matric suction equalization stage) and at the end of shearing stage can be predicted using Eqs. (15) and (19), respectively.

For the prediction of shearing-infiltration test, the prediction of consolidation stage, matric suction equalization stage, and shearing stage of the shearing-infiltration tests were similar to the prediction of CD triaxial tests. For the infiltration stage, an increment in matric suction (Δs) of 0.5 kPa was applied while the net mean stress and deviator stress were maintained constant. For each infiltrating step, the corresponding yield stress, yield suction at isotropic stage were calculated based on the consistency condition (i.e., Eqs. (30) and (31)). The LC and SI yield curves at the beginning of the shearing stage and at the end of infiltration stage can be predicted using Eqs. (15) and (19), respectively.

4.3. Comparison with experimental results

4.3.1. Comparison of predicted yield curve with measured yield stress on the $p-s$ plane

The yield suctions obtained from SWCC tests and the yield stresses obtained from isotropic consolidation tests

were compared with the corresponding yield curve on the $p-s$ plane at the end of the consolidation stage for the SWCC tests and at the end of matric suction equalization stage for the isotropic consolidation tests predicted by the proposed equations in this study and the equations proposed by Alonso et al. (1990).

Fig. 11 shows the corresponding yield curves at the end of consolidation stage of the SWCC tests and the corresponding yield curves at the end of matric suction stage of the isotropic consolidation tests that were obtained from prediction using the equations proposed in this study, together with the yield suction obtained from SWCC tests and the yield stress obtained from isotropic consolidation tests. Fig. 12 shows the corresponding yield curves at the end of consolidation stage of the SWCC tests and the corresponding yield curves at the end of matric suction stage of the isotropic consolidation tests that were obtained from prediction using the equations proposed by Alonso et al. (1990), together with the yield suction obtained from SWCC tests and the yield stress obtained from isotropic consolidation tests. This figure indicated that plastic strain developed during the matric suction equalization stage of the IC-30, IC-50, and IC-300 tests since the SWCC test at net mean stress of 10 kPa gave the yield suction of 18 kPa. As a result, the yield stress obtained from the isotropic consolidation tests do not belong to the same LC yield curve. Similarly, plastic strain developed during the consolidation stage of the SWCC-50, SWCC-100, and SWCC-250 tests since the isotropic consolidation test at matric suction of 0 kPa showed that the yield stress was 25 kPa. As a result, the yield stress obtained from SWCC tests do not belong to the same SI yield curve. In addition, the predictions based on the equations proposed in this study (Fig. 11) are in closer agreement with the experimental data as compared to the predictions based on the Alonso et al. (1990) equations (Fig. 12). This could be attributed to the fact that the change in matric suction and hysteresis of SWCCs were incorporated in the proposed equations to provide better prediction of yield conditions under a certain matric suction and net mean stress in unsaturated soils.

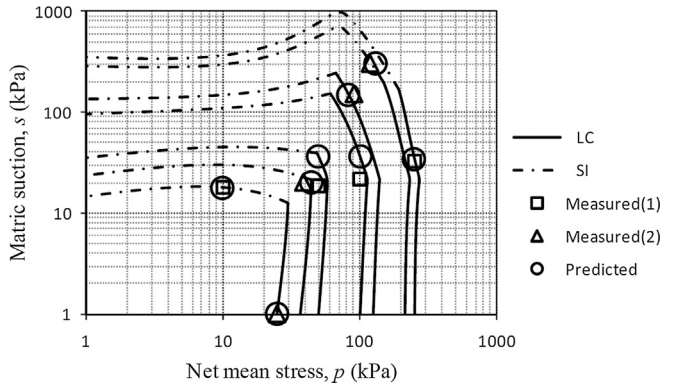

Fig. 11. Yield stresses and yield matric suctions obtained from laboratory test (measured 1: SWCC tests; measured 2: isotropic consolidation tests), and predicted yield curves based on the equations proposed in this study.

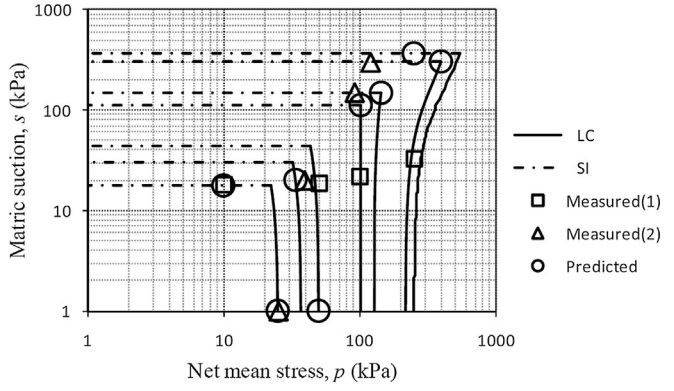

Fig. 12. Yield stresses and yield matric suctions obtained from laboratory test (measured 1: SWCC tests; measured 2: isotropic consolidation tests), and predicted yield curves based on the equations proposed by Alonso et al. (1990).

4.3.2. Comparison of predictions with the results from CD triaxial tests

The comparison between the predicted and measured results for consolidated drained tests at matric suctions of 100 kPa and 200 kPa under net confining stress of 300 kPa are presented in Fig. 13. The figure shows that at

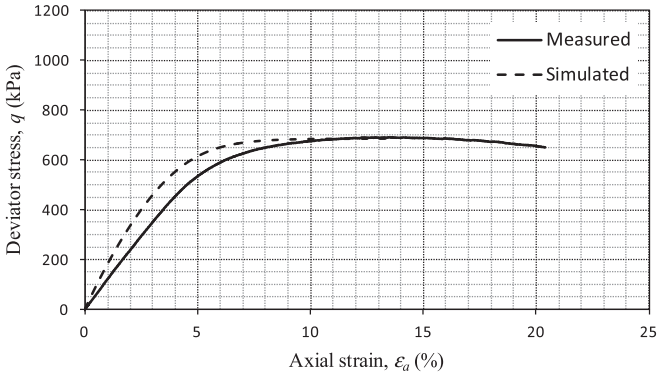

(a) Matric suction of 100 kPa and net confining stress of 300 kPa

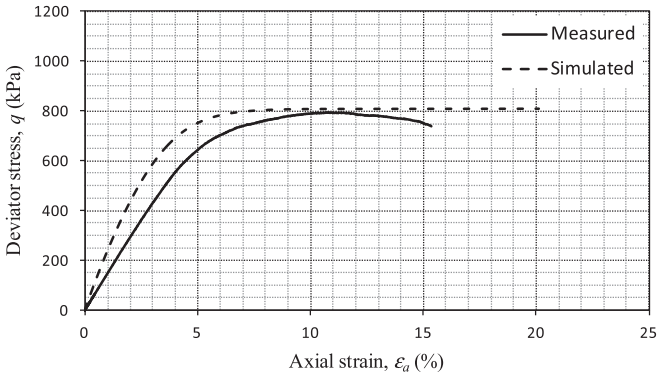

(b) Matric suction of 200 kPa and net confining stress of 300 kPa

Fig. 13. Comparison between predicted and measured results of the deviator stress versus axial strain during shearing stage for consolidated drained tests.

low axial strains, the deviator stress obtained from the model prediction is higher than the measured values. As axial strain increases, the difference between the predicted and the measured values decreases and both reach the same value at high axial strains. Fig. 14 shows the comparison between the predicted and measured results of volumetric strain during the shearing stage for consolidated drained tests at matric suctions of 100 kPa and 200 kPa under net confining stress of 300 kPa. Although the predicted results show stiffer behavior than the measured results, a reasonably good agreement of stress–strain relationships (especially yield deviator stresses) and volumetric strain during the shearing stage of consolidated drained tests is obtained between the predicted and measured results. The final value of M_* from shearing tests under consolidated drained conditions at matric suctions of 100 kPa and 200 kPa and under net confining stress of 300 kPa are 1.272 and 1.346, respectively. Fig. 15 shows the LC and SI yield curves at the beginning of the shearing stage and at the end of shearing stage together with the projection of yield path on the $p-s$ plane during shearing stage for consolidated drained test under net confining stress of 300 kPa at matric suction of 100 kPa.

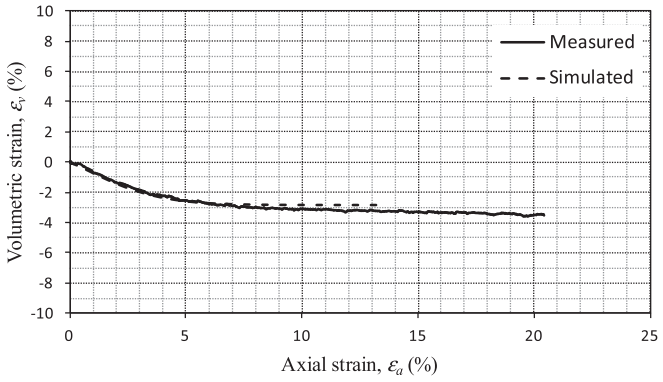

(a) Matric suction of 100 kPa and net confining stress of 300 kPa

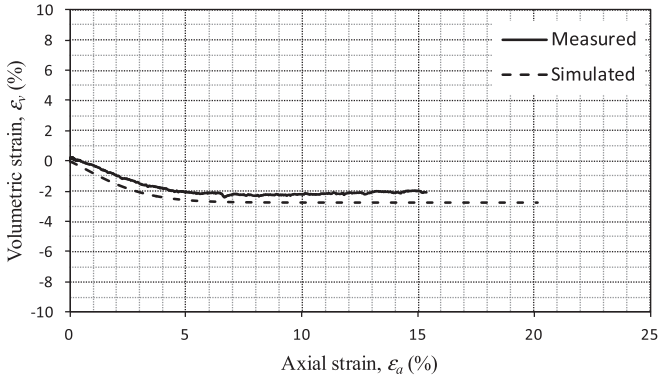

(b) Matric suction of 200 kPa and net confining stress of 300 kPa

Fig. 14. Comparison between predicted and measured results of the volumetric strain versus axial strain during shearing stage for consolidated drained tests.

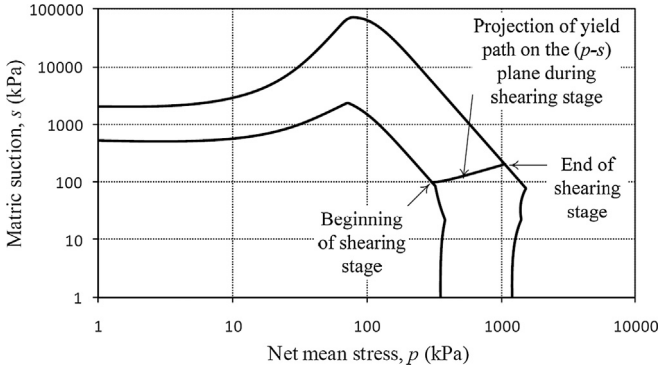

Fig. 15. Yield curve at the beginning of the shearing stage and at the end of shearing stage together with the projection of yield path during the shearing stage for consolidated drained test under net confining stress of 300 kPa at matric suction of 100 kPa.

4.3.3. Comparison of predictions with the results from shearing-infiltration tests

The results obtained from the model prediction and the experiments for shearing infiltration tests are presented in Figs. 16–18. Similar to the case of consolidated drained tests (Fig. 13) at low axial strains, the deviator stress

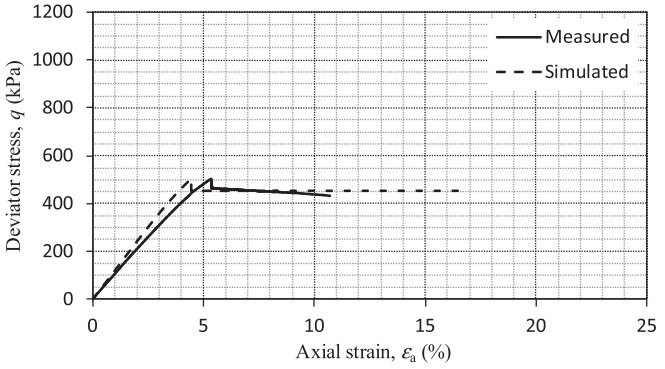

Fig. 16. Comparison between predicted and measured results of the deviator stress versus axial strain during shearing and infiltration stage for shearing infiltration test at initial matric suction of 200 kPa and net confining stress of 200 kPa.

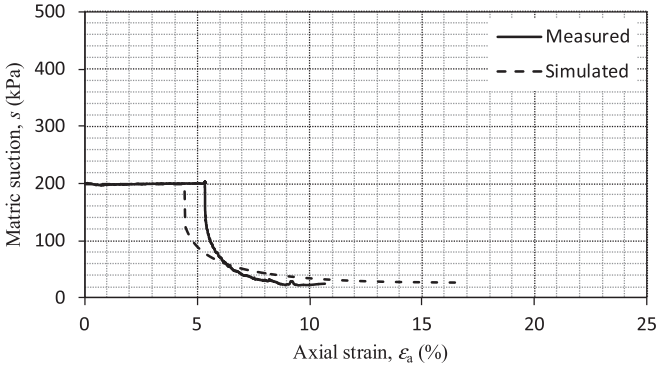

Fig. 17. Comparison between predicted and measured results of the matric suction versus axial strain during shearing and infiltration stage for shearing infiltration test at initial matric suction of 200 kPa and net confining stress of 200 kPa.

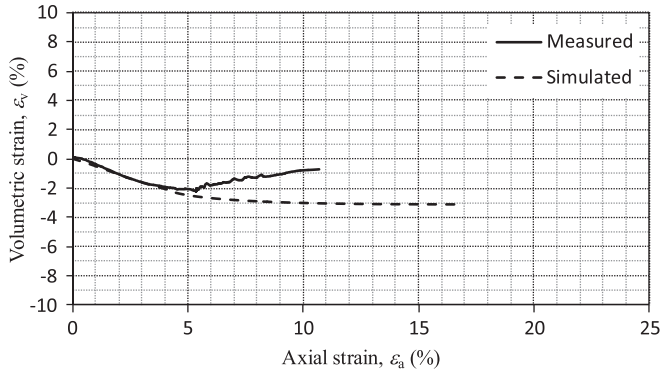

Fig. 18. Comparison between predicted and measured results of the volumetric strain versus axial strain during shearing and infiltration stage for shearing infiltration test at initial matric suction of 200 kPa and net confining stress of 200 kPa.

obtained from the model prediction is higher than the measured values (Fig. 16). Therefore, at the same deviator stress at the end of the shearing stage, the axial strain obtained from the prediction is lower than the one observed from the experiment. The relationship between matric suction and axial strain in Fig. 17 shows that the axial strain starts to increase gradually at the same matric suction (i.e., 75 kPa) as observed in the experiment and predicted by the proposed model. In other words, failure occurred at the same matric suction (i.e., 75 kPa) during the experiment and as predicted by the proposed model. Fig. 18 shows the relationship between volumetric strain and axial strain obtained from the prediction and shearing-infiltration tests. The predicted volumetric strain shows a good agreement with the experimental results when the axial strain is smaller than 5%. There are discrepancies between the predicted and measured results of volumetric strain when the axial strain is higher than 5%. These discrepancies could be attributed to the injected water from the base of the soil specimen. The injected water contributed to dilative behavior of the soil that cannot be simply predicted through the proposed model in an idealized condition. Although the proposed model has such limitation, the general trend of the measured stress–strain relationship, matric suction variation, volumetric strain of the soil specimen is fairly well predicted. The final value of M_{ast} from shearing tests under shearing-infiltration conditions at matric suction of 200 kPa and net confining stress of 200 kPa is 1.258. Fig. 19 shows the LC and SI yield curves at the beginning of the shearing stage, at the end of the shearing stage, and at the end of the infiltration stage together with the projection of yield paths on the $p-s$ plane during shearing stage and infiltration stage for shearing-infiltration test under net confining stress of 200 kPa at matric suction of 200 kPa.

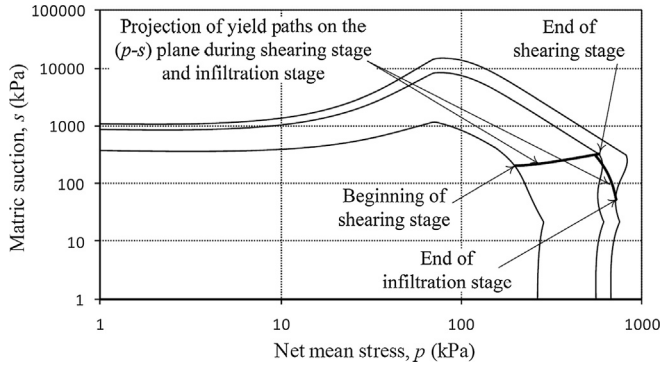

Fig. 19. Yield curve at the beginning of the shearing stage, at the end of the shearing stage and at the end of infiltration stage together with the projection of yield paths during the shearing stage and infiltration stage for shearing-infiltration test under net confining stress of 200 kPa at matric suction of 200 kPa.

5. Conclusions

The conclusions from this study are summarized as follows:

(1) The elasto-plastic constitutive relations were successfully developed by introducing the suction increase (SI) yield curve. In addition, the yield surface in $p-q-s$ space and the relationships between specific water volume, matric suction and net mean stress were proposed. The change in specific water volume can be caused by the change in net normal stress, deviator stress or matric suction. The influence of hysteresis is taken into account in the proposed model.
(2) The prediction of yield curves on $p-s$ plane (i.e., LC and SI yield curves) based on the proposed model showed a closer agreement with the experimental data obtained from SWCC tests and isotropic consolidation tests of compacted kaolin as compared to the predictions based on Alonso et al. (1990) model.
(3) In addition, the predicted and the measured shear strengths are in good agreement while the predicted volume change was partly in agreement with the measured volume change.
(4) The proposed model can be used to solve the hydro-mechanical behavior of unsaturated soils (e.g., kaolin) under steady-state and transient conditions.

References

Alonso, E.E., Gens, A., Hight, D.W.A., 1987. Special Problem Soils. In: Proceedings of the 9th European Conference on Soil Mechanics and Foundation Engineering, Dublin, Vol. 3, pp. 1087–1146.
Alonso, E.E., Gens, A., Josa, A., 1990. A constitutive model for partially saturated soils. Géotechnique 40, 405–430.
Bolzon, G., Schrefler, B.A., Zienkiewicz, O.C., 1996. Elasto-plastic soil constitutive laws generalized to partially saturated states. Géotechnique 46, 279–289.
Chiu, C.F., Ng, C.W.W., 2003. A state-dependent elasto-plastic model for saturated and unsaturated soils. Géotechnique 53, 809–829.
Cui, Y.J., Delage, P., 1996. Yielding and plastic behavior of unsaturated silt. Géotechnique 46, 291–311.
Delage, P., Graham, J., 1995. "Understanding the behaviour of unsaturated soils requires reliable conceptual models. In: Proceedings of the

1st International Conference on Unsaturated Soils, Paris, vol. 3, pp. 1223–1256.
Fredlund, D.G., Rahardjo, H., 1993. Soil Mechanics for Unsaturated Soils. John Wiley and Sons Inc., New York.
Fredlund, D.G., Xing, A., Fredlund, M.D., Barbour, S.L., 1996. The relationship of the unsaturated soil shear strength to the soil-water characteristic curve. Can. Geotech. J. 33 (3), 440–448.
Gens, A., Alonso, E.E., 1992. A framework for the behaviour of unsaturated expansive clays. Can. Geotech. J. 29, 1013–1032.
Gens, A., Potts, D.M., 1982. A theoretical model for describing the behaviour of soils not obeying Rendulic's principle. In: Proceedings of 1st Syposium on Numerical Modelling Geomechanics, Zurich, pp. 312–323.
Han, K.K., 1997. Effect of hysteresis, infiltration and tensile stress on the strength of unsaturated soil. PhD Thesis, School of Civil and Structural Engineering, Nanyang Technological University, Singapore.
Head, K.H., 1986. Manual of Soil Laboratory Testing. John Wiley and Son Inc, New York, vol. 3, pp. 942–945.
Hilf, J.W., 1956. An Investigation of Pore-Water Pressure in Compacted Cohesive Soils. PhD Thesis, Tech. Memo. No. 654. U.S. Dept. of Interior, Bureau of Reclamation, Design and Construction Division, Denver, CO654.
Kim, Y., Jeong, S., Kim, J., 2016. Coupled infiltration model of unsaturated porous media for steady rainfall. Soils Found. 56 (6), 1071–1081.
Meilani, I., Rahardjo, H., Leong, E.C., 2005. Pore-water pressure and water volume change of an unsaturated soil under infiltration conditions. Can. Geotech. J. 42 (6), 1509–1531.
Ohmaki, S., 1982. Stress-strain Behaviour of Anisotropically, Normally Consolidated Cohesive Soil. In: Proceedings of 1th Syposium on Numerical Modelling Geomechanics, Zurich, pp. 260–269.
Rampino, C., Macuso, C., Vinale, F., 1999. Mechanical behavior of an unsaturated dynamically compacted silty sand. Ital. Geotech. J. 33 (02), 26–39.
Rampino, C., Mancuso, C., Vinale, F., 2000. Experimental behaviour and modelling of an unsaturated compacted soil. Can. Geotech. J. 37, 748–763.
Reddy, B.V.V., Jagadish, K.S., 1993. The static compaction of soils. Géotechnique 43 (2), 337–341.
Sheng, D., Fredlund, D.G., Gens, A., 2008. A new modeling approach for unsaturated soils using independent stress state variable. Can. Geotech. J. 45, 511–534.
Simoni, L., Schrefler, B.A., 2001. Parameter identification for a suction-dependent plasticity model. Int. J. Numer. Anal. Meth. Geomech. 25, 273–288.
Tang, G.X., Graham, J., 2002. A possible elasto-plastic framework for unsaturated soils with high plasticity. Can. Geotech. J. 39, 894–907.
Thomas, H.R., He, Y., 1994. Analysis of coupled heat moisture and air transfer in a deformable unsaturated soil. Géotechnique 44 (5), 677–689.
Thu, T.M., Rahardjo, H., Leong, E.C., 2007a. Elastoplastic model for unsaturated soil with the incorporation of soil-water characteristic curve. Can. Geotech. J. 44, 67–77.
Thu, T.M., Rahardjo, H., Leong, E.C., 2007b. Soil-water characteristic curve and consolidation behavior of a compacted silt. Can. Geotech. J. 44 (3), 266–275.
Thu, T.M., Rahardjo, H., Leong, E.C., 2007c. Critical state behaviour of a compacted silt. Soils Found. 47 (4), 749–755.
Toll, D.G., 1990. A framework for unsaturated soils behaviour. Géotechnique 40, 31–44.
Vanapalli, S.K., Fredlund, D.G., Pufahl, D.E., Clifton, A.W., 1996. Model for the prediction of shear strength with respect to soil suction. Can. Geotech. J. 33, 379–392.
Wang, Q., Pufahl, D.E., Fredlund, D.G., 2002. A study of critical state on an unsaturated silty soil. Can. Geotech. J. 39, 213–218.
Wheeler, S.J., Sivakumar, V., 1995. An elasto-plastic critical state framework for unsaturated soil. Géotechnique 45, 35–53.
Wheeler, S.J., 1996. Inclusion of specific water volume within an elasto-plastic model for unsaturated soil. Can. Geotech. J. 33, 42–57.
Wheeler, S.J., Sharma, R.S., Buisson, M.S.R., 2003. Coupling of hydraulic hysteresis and stress-strain behaviour in unsaturated soil. Géotechnique 53, 41–54.